Single-cell Data Unveil the Multifaceted Role of LRP1 in Alzheimer's Disease Pathogenesis

Kang Chen

Academy of Military Medical Sciences, Academy of Military Sciences

ZiLin Wei

Academy of Military Medical Sciences, Academy of Military Sciences

AiLi Wei

Academy of Military Medical Sciences, Academy of Military Sciences

YingKai Qin

Academy of Military Medical Sciences, Academy of Military Sciences

Chen Liu

Academy of Military Medical Sciences, Academy of Military Sciences

Haolin Xin

Academy of Military Medical Sciences, Academy of Military Sciences

Shisheng Chen

Academy of Military Medical Sciences, Academy of Military Sciences

Yi Ge

Information Center of Logistics Support Department of CMC

Bin Li

No. 950 Hospital of the Chinese People's Liberation Army

Kun Wang

Academy of Military Medical Sciences, Academy of Military Sciences

TianHui Wang (✉ wydny668@163.com)

Academy of Military Medical Sciences, Academy of Military Sciences

Case Report

Additional Declarations: No competing interests reported.

Abstract

Background

The role of low-density lipoprotein receptor-related protein 1 (LRP1) in Alzheimer's disease (AD) has been a focal point of research, highlighting its crucial function in amyloid-beta (Aβ) metabolism in the central nervous system. Despite these significant findings, the detailed mechanisms of LRP1 in neuronal Aβ handling and its systemic effects in AD have not been fully elucidated. Here, we employ innovative single-cell data analysis and temporal analysis complemented by multi-tissue data integration to shed light on the specific roles and systemic impact of LRP1 in AD.

Methods

We conducted in-depth single-cell data mining and analysis using publicly available datasets from the GSE181279, GSE174367, and GSE173429. These findings were augmented with complementary in vivo and in vitro experiments aimed at substantiating the function of LRP1 in the phagocytosis of Aβ by hepatic macrophages.

Results

Detailed data mining and analysis of public datasets have revealed the nuanced role of LRP1 in AD, notably impacting the brain, blood, and liver. Our findings demonstrated pronounced upregulation of LRP1 in brain astrocyte, microglia, and oligodendrocyte progenitor cells (OPCs), establishing a direct correlation with the neurological manifestations of AD. In peripheral blood mononuclear cells (PBMC), LRP1 exhibited unique expression patterns, underscoring its systemic influence on AD pathology. Critically, our data reveal that physical exercise modulates LRP1 expression in Kupffer cells, identifying lifestyle factors as key modulators of the molecular processes involved in AD. Experimental evidence further confirms that reduced LRP1 expression is associated with impaired amyloid-beta clearance, highlighting its pivotal role in the progression of AD. Collectively, these insights position LRP1 as a central molecular player in AD, suggesting novel avenues for therapeutic intervention.

Conclusions

This study, which involved leveraging multi-tissue single-cell analyses of human and mice samples, investigated the multifaceted functionality and molecular dynamics of LRP1 in AD progression. Additionally, this study unveiled the modulatory effects of physical exercise on LRP1 expression, paving the way for novel therapeutic approaches for AD management.

Introduction

AD, a progressive neurodegenerative disorder, is a significant global health challenge[1−3]. Central to AD pathophysiology is the accumulation of Aβ plaques[4, 5], which is implicated in neuronal damage and cognitive decline[6, 7]. Despite extensive research, significant gaps exist in our understanding of the

molecular mechanisms underlying Aβ clearance and the progression of AD[8−10]. Recent findings have indicated a potential link between LRP1 expression and Aβ clearance in various tissues[11, 12], including the liver and brain. However, the inter- and intracellular heterogeneity of LRP1 expression among tissues, together with its impact on AD progression, have not been determined. This lack of clarity is crucial, as elucidating the mechanisms of Aβ clearance could lead to novel therapeutic approaches for AD. This study specifically focused on the role of LRP1, a key player in Aβ clearance[13−16].

Our study aimed to provide a comprehensive analysis of the expression and function of LRP1 across multi-tissue, with a specific focus on the brain, blood, and liver in AD patients. Exploring the impact of physical exercise on LRP1 expression[17], we investigated the subsequent effects of physical exercise on immune cell functionality within the AD context. Utilizing single-cell RNA data from multi-tissue [18−20], our objective was to elucidate the complex role of LRP1 in AD, thereby enhancing our understanding of its potential as a therapeutic target.

In our study, we provided significant insights into the involvement of LRP1 in AD, revealing distinct expression patterns across multi-tissue (brain, blood, and liver). We demonstrated the modulation of LRP1 by physical exercise and its systemic influence on AD progression, highlighting its potential as a key target for therapeutic intervention.

Materials and Methods

Availability of Data

The public mice and human AD scRNA-seq data used in this study can be downloaded from the Gene Expression Omnibus under accession numbers GSE181279[18], GSE174367[19] and GSE173429[20].

Single-cell RNA-seq data processing

The single-cell gene expression count matrices were analyzed by the Seurat R package[21] (version 4.4.0). Cells with no less than 400 genes and no more than 10% mitochondrial genes were retained. The filtered expression matrices were normalized to the total number of UMIs per cell and $\log_2$-transformed. Scaled data from all cells were subjected to principal component analysis (PCA) of highly variable genes. The first 15 principal components and 500 neighbors were used for UMAP embedding, and the first 2 principal components were used for UMAP initialization. Different cell types were isolated and subjected to PCA and UMAP for further analysis. Cell type annotation was performed using the single R package[22] (version 2.0.0), and the data were refined via manual annotation. The marker genes of each cell cluster were identified by the FindAllMarkers function, with min.pct = 0.25 and thresh.use = 0.25. Differentially expressed genes (DEGs) were identified with the FindAllMarkers function in Seurat. Differences in expression between each cell cluster and others larger than 0.3 were set as the threshold for significantly differential expression.

Functional enrichment analysis

GO enrichment analysis was performed using the enrich GO function in the clusterProfiler R package[23] (version 4.9.0). Kyoto Encyclopedia of Genes and Genomes (KEGG) enrichment analysis was performed using the enrich KEGG function in the clusterProfiler R package (version 4.9.0). GSEA was performed using the gseGO function in the clusterProfiler R package (version 4.9.0).

Quantifying gene set activity within cells

To quantify gene set activity within individual cells, we performed a gene set variation analysis (GSVA) using the GSVA R package[24] (version 1.46.0) with the following categories: "C5" and subcategory= "BP". The AUCell R package (version 1.20.2) was used to compute gene expression rankings based on the area under the curve (AUC) value derived from model genes. Furthermore, the UMAP embedding of each cell's AUC was visually represented using the ggplot2 R package[25] (version 3.4.4).

Cell–cell communication analysis

Cell–cell communication was determined with the CellChat R package[26] (version 1.6.1). Differentially expressed signaling genes (P< 0.05) were first identified across cell clusters in the scRNA-seq dataset to infer specific cellular communications. Next, signaling sources, influencers, targets and higher-order information were obtained via social network analysis.

Clustering genes based on expression changes

Mfuzz[27] (version 2.50.0) was used to cluster the DEGs between disease stages. Pseudo-bulk gene expression changes across all cells and time points were determined by calculating the average expression of each gene at every time point. This procedure yielded an n gene by m time point matrix, with n representing the number of DEGs and m representing the number of time points in each dataset. Genes exhibiting similar changes in expression throughout development were grouped using Mfuzz-generated gene clusters. For each cluster, we assigned a gene order score by calculating the Pearson correlation score of the gene expression trends with the cluster's center expression score provided by Mfuzz. The resulting gene order score ranged from 0 to 1.

Animals and groups

The animal study was reviewed and approved by the Institutional Animal Care and Use Committee (IACUC) of the Chinese Academy of Military Medical Science. A total of 16 C57BL/6 male mice and 16 APP/PS1 male mice (12 weeks of age, weighing 21–25 g/animal; Beijing HFK Bioscience Co., Ltd.) were housed in eight cages (8 mice/cage) under conventional conditions (at a temperature of 16–20°C and a relative humidity of 40–70%) with a regular 12-h light:12-h dark cycle (with lights on at 8:00 am). All mice had free access to food and water. After seven days of adaptive feeding, the mice were randomly divided into four groups: the white control group (WTC, n = 8), white exercise group (WTE, n = 8), APP/PS1 control group (ADC, n = 8), and APP/PS1 exercise group (ADE, n = 8).

Aerobic Exercise Protocol

In alignment with established protocols[28], our aerobic exercise regimen involved swimming training in an opaque prototype plastic bucket (500 mm upper caliber, 400 mm lower caliber, 620 mm height), with the water temperature consistently maintained at 31 ± 1°C. To acclimatize the mice to this regimen, the exercise group underwent a five-day preliminary swimming period, beginning at 10 minutes on the first day and increasing incrementally by 10 minutes daily, culminating in 50 minutes on the fifth day. The formal 12-week experiment comprised daily 50-minute freely swimming sessions from Monday to Friday, conducted between 19:00 and 21:00. To control for environmental stress, no exercising mice were placed on a flat open surface within the swimming pool for equivalent durations. After swimming, the mice were gently dried with a towel to mitigate stress from body temperature regulation.

Novel Object Recognition Test

Following the 12-week aerobic exercise intervention, the spatial learning and memory abilities of the mice were evaluated using the Novel Object Recognition (NOR) Test, facilitated by Tracking Master-NOR (Shanghai Xinruan Information Technology Co., Ltd., Shanghai, China). The experimental setup comprised a square box (40 × 40 cm base, 40 cm height) in gray, featuring a novel object and a camera for observation. The test entailed a training phase in which mice were introduced to two identical objects within the setup for a 5-minute exploration period. This was followed by a testing phase in which one of the previously encountered objects was replaced with a new object, during which the mice were allowed another 5 minutes of free exploration. To prevent olfactory interference, the setup was cleansed with 75% ethanol after each session. The assessment of memory and recognition capabilities was based on analyzing the proportion of time the mice spent interacting with the old and new objects.

Morris water maze test

Subsequent to the NOR test, we employed the water maze test to further evaluate the spatial learning and memory abilities of the mice in each group. This was performed using the Tracking Master-MWM system (Shanghai Fanbi Intelligent Technology Co., Ltd., Shanghai, China). The experimental setup included a transparent plastic platform submerged 1.5 cm beneath the water surface in the maze's first quadrant, serving as a hidden platform for the mice to locate. The maximum escape latency was set at 60 seconds. The escape latency of mice successfully locating and remaining on the platform for 3 seconds within this timeframe was also recorded. In cases where the mouse failed to find the platform within 60 seconds, the escape latency was automatically set at the maximum limit. The testing protocol entailed four daily positioning navigation trials from different sides of the tank, spanning all four quadrants of the water maze, over the initial five days. This rigorous schedule was designed to assess the progressive development of spatial learning abilities in the mice. On the sixth day, the experiment shifted to a spatial exploration test by removing the hidden platform. Mice were introduced to the water from the tank's third quadrant to evaluate spatial memory.

Western blot

The aim of this Western blot analysis was to assess the levels of LRP1 and Aβ in mouse liver tissues. To begin the experiment, liver tissues were homogenized in 500 μL of a specially prepared protein lysis

buffer for each sample, ensuring efficient cell disruption and protein extraction. The lysis buffer used was composed of RIPA buffer, phosphatase inhibitor, and protease inhibitor at a 970:20:10 ratio and was optimized to protect and preserve the integrity of the proteins. Following homogenization, the mixture was incubated at -40°C to promote complete lysis of the tissue samples. This process separated the supernatant, which was subsequently transferred to new EP tubes for further analysis. The protein concentrations in the supernatants were determined using a BCA Protein Assay Kit (PC002; Solarbio, China) according to the manufacturer's instructions. After quantification, the proteins were denatured in a 100°C water bath for 10 minutes. The denatured proteins were then separated using 10% SDS−PAGE and subsequently transferred onto PVDF membranes. For blocking, the membranes were incubated with 5% skim milk powder in TBST for 2 hours at room temperature. This step was crucial for preventing nonspecific binding. Next, the membranes were incubated overnight at 4°C with primary antibodies against LRP1 (Abcam, ab92544, 1:5000 dilution) and Aβ (Proteintech Group, 60342-1-Ig, 1:1000 dilution), both of which were diluted in TBST containing 5% skim milk powder. GAPDH (Proteintech Group, 10494-1-AP, 1:5000 dilution) was used as a loading control. Following the primary antibody incubation, the membranes were washed six times with TBST for 5 minutes each to eliminate unbound primary antibodies. Subsequently, the sections were incubated for 1 hour at room temperature with HRP-conjugated goat anti-rabbit or HRP-conjugated goat anti-mouse secondary antibodies (Proteintech Group, American, 1:5000 dilution). After secondary antibody incubation, the membranes were washed six times with TBST to remove any residual antibodies. The final step involved detecting protein expression levels using the Immobilon Western Chemiluminescent HRP Substrate (Thermo et al.). The grayscale values of the target protein bands were analyzed using ImageJ software, which provided quantitative data on the levels of LRP1 and Aβ in the liver tissue samples.

ELISA

At the end of the behavioral assay, whole blood was collected from 5 mice per group. This was followed by centrifugation at 3000 rpm for 10 min to obtain plasma. Concentrations of $A\beta_{40}$ and $A\beta_{42}$ were then quantified according to the ELISA kit protocol. Importantly, each sample was analyzed in triplicate to ensure accuracy and consistency.

Cell culture and treatment

RAW 264.7 cells, sourced from Pricella (China), were cultured in DMEM supplemented with 10% FBS, providing optimal conditions for cell growth. To explore the functional role of LRP1, we employed siRNA-mediated gene silencing. RAW 264.7 cells were transfected with 20 nM LRP1-targeting siRNA using RNATransMate transfection reagent following the manufacturer's protocol. The cells were incubated at 37°C in a 5% CO_2 incubator. After 24 hours, the cells were harvested for LRP1 knockdown efficiency analysis using both fluorescence microscopy and Western blotting. Concurrently, a control group was treated with FAM-labeled nontargeting control siRNA (FAM-NC, 20 nM) for 24 hours. The siRNA sequences used were as follows: LRP1 (mouse) siRNA: 5'-GCGAACAAAUACACUGGCUAATT-3', and FAM-NC siRNA: 5'-UUCUCCGAACGUGUCACGUTT-3'.

Aβ uptake assay

For the Aβ uptake assay, RAW 264.7 cells were seeded at a density of 100,000 cells per well in a 24-well plate. The following day, the culture medium was replaced, and the cells were transfected with LRP1 siRNA using RNATransMate to knock down LRP1 expression. After 24 hours, the cells were treated with the $Aβ_{25-35}$ peptide (MedChemExpress, HY-P0128, 500 nM) for 1 hour at 37°C following the manufacturer's instructions. After treatment, the cells were washed three times with PBS, after which immunofluorescence staining was performed. Experiments were conducted in triplicate, and the data from the blank control group were normalized to aggregate datasets from multiple experimental replicates.

Immunofluorescence

Mice were perfused with 4% paraformaldehyde for 15 minutes at room temperature. Then, the brain tissue was further fixed with the same concentration of 4% paraformaldehyde and embedded in paraffin. For the immunofluorescence method, first, sections were deparaffinized, and then antigen retrieval was performed. For cellular immunofluorescence staining, cell slides were directly fixed with 4% paraformaldehyde. Then, the brain sections or cell slides were blocked and permeabilized in 1% BSA for 60 min and subsequently incubated with primary antibodies overnight at 4°C, anti-LRP1 (Abcam, ab92544, 1:100) and anti-beta amyloid (Boster, MA00081, 1:200). Next, the sections and cell slides were washed three times with PBS (pH = 7.4) for 5 minutes each. Then, the sections were incubated with the corresponding fluorescent secondary antibodies in the dark at room temperature for 1 hour with Alexa Fluor® 488 (Abcam, ab150077, 1:200) and Alexa Fluor® 647 (Abcam, ab150115, 1:200). Afterwards, the sections and cell slides were again washed three times with PBS (pH = 7.4) for 10 minutes each. Then, the cells were stained with DAPI solution (Solarbio, C0065) at room temperature for 5 minutes. Finally, the sections and cell slides were washed three additional times with PBS (pH = 7.4) for 5 minutes each. Subsequently, the target antibody and nuclear fluorescence were observed under a fluorescence microscope, and the samples were sealed with an anti-fluorescence quenching agent. Finally, the fluorescence intensity was quantified using ImageJ software.

Statistical analysis

Bioinformatics analysis

Statistical analyses and data processing for the bioinformatics part of the study were conducted on the R platform (version 4.2.2). Relative gene expression levels between the case and control groups were compared using the nonparametric Wilcoxon signed-rank test. To explore the differential expression of key genes across various disease stages, we employed the Games-Howell test, ensuring a 95% confidence interval. All bioinformatics quantifications and analyses were conducted in a blinded manner, and the sample conditions were not met by the analysts.

Molecular Biology Validation

For the molecular biology validation part of the study, all the statistical analyses were performed using GraphPad Prism 9.0 (GraphPad Software, Inc., USA). The data are presented as the means ± SEMs, unless otherwise specified in the figure legends. To assess the differences between datasets, we employed two-way ANOVA followed by a Bonferroni post hoc correction, Student's paired t test, or the paired Wilcoxon test for nonparametric data. The threshold for statistical significance was set at $*P < 0.05$, $**P < 0.01$, $***P < 0.001$, and $****P < 0.0001$.

Results

Charting LRP1's Regulatory Role in Astrocyte Diversity During AD Progression

We collected published scRNA-seq datasets from both mice and human AD samples to explore the role of LRP1 in different stages of AD at singleS-cell resolution. We first used the scRNA-seq dataset to determine the regulatory role of LRP1 in astrocyte, which included 54,104 cells after quality control [19]. The lineages were annotated based on the R package (version 4.4.0). We observed that LRP1 expression was notably elevated in astrocyte, microglia, and OPCs (Fig. 1A), which was consistent with prior findings on the role of astrocyte and microglia in Aβ protein phagocytosis[29–31]. On the basis of our reclustering analysis of the astrocyte subtypes (Fig. 1A), we found that LRP1 was highly expressed in A0 cells (Fig. 1B). Further exploring the heterogeneity in astrocyte cell composition between different stages of A0, we observed that with the progression of the disease, LRP1 was highly expressed in stage 5 patients (Fig. 1G). Therefore, we focused on analyzing the characteristics of A0 in Stage 5 and the functions of LRP1. We identified 1040 DEGs (log2FC > 0.4, cell proportion > 0.3) between Stages 2, 5, and 6 and Stage 1 through FindMarker analysis, including 381 upregulated and 659 downregulated genes (Fig. 1C). To compare the differences between stages, we conducted functional enrichment analysis and Mfuzz coexpression analysis for these DEGs (Fig. 1D-F). Specifically, we performed a GSEA of DEGs in Stage 5 vs Stage 1 (log2FC > 0.5, cell proportion > 0.1) and found that learning and memory functions were activated in Stage 5 compared to Stage 1 (Fig. 1D). To further explore the functions of these DEGs, we performed a Gene Ontology (GO) analysis (Fig. 1H), which revealed that the primary functions related to LRP1 include receptor-mediated endocytosis and extracellular matrix regulation, while AD-related functions mainly involve cognition, memory, and neural development. Additionally, we conducted a GSEA of DEGs in Stage 6 vs Stage 1 (log2FC > 0.5, cell proportion > 0.1), which showed that acute inflammatory response functions were activated in Stage 6 compared to Stage 1. To further explore the heterogeneity of LRP1 in different stages of A0, we analyzed the DEGs across different stages using Mfuzz and found that LRP1 was clustered in cluster 6 (Fig. 1F). To more precisely delineate the functions of A0, we performed GSVA[32, 33], which showed that functions related to acute inflammation and cell apoptosis trended upward with the progression of AD (Fig. 1I). Aβ clearance was activated in Stage 5 and inhibited in Stage 6, while functions such as neuronal differentiation and other neural activities were suppressed in Stages 5 and 6.

Charting LRP1's Regulatory Role in Microglial Diversity During AD Progression

We focused on the primary functions of astrocyte in A0. Similarly, for microglia, we applied a straightforward analytical approach. To understand the roles of LRP1 in AD, we initially performed a reclustering analysis on microglia (Fig. 2A) by selecting M0, a subtype that expresses LRP1 across all stages of the disease (Fig. 2B). Our objective was to elucidate the expression and mechanisms of LRP1 in M0 macrophages as AD progresses. To this end, we conducted a differential analysis of LRP1 expression in M0 macrophages across different stages (Fig. 2C) and found that LRP1 was highly expressed specifically in stages 2 and 5. Since stage 2 was classified as a control group in the original study, we focused our analysis on the characteristics of stage 5 patients and the functions involving LRP1. Using FindMarkers, we compared stages 2, 5, and 6 with stage 1 (Supplementary Fig. 1A), identifying 2211 DEGs (log2FC > 0.4, cell proportion > 0.3), 951 of which were upregulated and 1260 of which were downregulated. To delineate the progression of AD, we conducted functional enrichment analysis and Mfuzz coexpression analysis for these DEGs (Fig. 2D-E). Moreover, we performed a GSEA of DEGs in Stage 5 vs Stage 1 (log2FC > 0.4, cell proportion > 0.1) and found that functions related to neurons and neural system development were activated in Stage 5 (Supplementary Fig. 1B). To further explore the functions of these DEGs, we conducted a GO analysis (Fig. 2E). The results revealed that the primary functions related to LRP1 include receptor-mediated endocytosis and Aβ protein clearance, while the main functions of AD-related proteins involve immune regulation. To further investigate the stage-specific roles of LRP1, we analyzed the DEGs using Mfuzz and found that LRP1 was clustered in cluster 4 (Fig. 2D). To refine our understanding of M0's functions, we performed a GSVA, which showed that Aβ clearance and memory functions were activated in Stage 5 and inhibited in Stage 6 (Fig. 2F). Subsequently, we characterized the interactions and communication relationships between microglia and astrocyte. We conducted a CCI analysis of all the cells to determine the differences in the APP pathway between microglia and astrocyte. Focusing on the APP pathway, we analyzed the ligand−receptor pair and found that the APP-CD74 gene plays a major contributing role (Fig. 2G). Previous studies have shown that the interaction between APP and CD74 can reduce Aβ protein deposition[34]. Interestingly, the key gene (receptor) CD74 identified by the CCI, which was highly expressed specifically in our focused M0 subtype (Fig. 2H), exhibited a decreasing trend in expression as the disease progressed (Supplementary Fig. 1C), suggesting that microglia play a reducing role in clearing Aβ protein deposition in later stages of the disease. Additionally, we found that the gene regulating Aβ protein deposition (APP) was also highly expressed in stage 5 (Fig. 2I), further demonstrating the importance of stage 5 in regulating the Aβ protein.

Charting LRP1's Regulatory Role in PBMC Diversity During AD Progression

To comprehensively understand the functional diversity of LRP1, we investigated its expression in PBMC [18]. The scRNA-seq dataset, which included 35,812 cells after quality control, was used to chart the

regulatory role of LRP1 in PBMC. The linages were annotated based on the Seurat R package (version 4.4.0). We observed five distinct cell clusters in PBMC (Fig. 3A), with LRP1 showing notable expression in monocytes (log2FC = 1.4), suggesting that LRP1 plays a key role in AD progression. A finer reclustering analysis with a resolution of 0.5 resulted in five subclusters, encompassing 16,382 genes across 441 samples (Fig. 3A). A more detailed reclustering analysis with a resolution of 0.5 resulted in five subclusters, encompassing 16,382 genes across 441 samples (Fig. 3A). Following a literature-reported reannotation[18] of monocytes, we pinpointed significantly elevated LRP1 expression in two specific subgroups: CD14 Mono_Activated (log2FC = 0.8) and CD14 Mono_HLA (log2FC = 0.35) (Fig. 3B-C). These disease-specific and control-specific populations exhibited similar expression profiles. Thus, we investigated the mechanistic role of LRP1 in AD, particularly focusing on the differential expression and functional implications between the CD14 Mono_Activated and CD14 Mono_HLA groups.

First, using a T test, we detected that LRP1 gene expression was significantly upregulated in CD14 Mono_Activated cells compared to CD14 Mono_HLA cells (P = 5.65e-03) (Fig. 3D). Additionally, we identified 702 DEGs (log2FC > = 0.5, cell proportion > 0.25) between these two groups using FindMarkers (Fig. 3E), including 429 upregulated and 273 downregulated genes. To gain deeper insights, we conducted functional enrichment analysis on these DEGs. The results revealed that AD-related functions mainly included neuronal death, acute inflammation, and oxidative stress, while LRP1-related functions primarily involved phagocytosis, Aβ protein clearance, and the neuroinflammatory response (Fig. 3F). To corroborate the phagocytic function of monocytes, we examined the expression levels of phagocytosis-related genes (CD36, LRP1, ITGAM, and PICALM) in monocytes. We found that these genes were highly expressed specifically in CD14 Mono_Activated cells (Fig. 3G), suggesting that monocyte function is primarily exerted by CD14 Mono_Activated cells. Furthermore, we performed GSEA on the DEGs (log2FC > 0.5, cell proportion > 0.25) (Fig. 3H). The results showed that functions such as monocyte proliferation, immune function, and neutrophil migration were suppressed. Then, using AUCell analysis, we revealed which biological processes or signaling pathways were activated (Fig. 3I). We found that Aβ clearance, negative regulation of the lipopolysaccharide-mediated signaling pathway, and positive regulation of the neuroinflammatory response were activated in both CD14 Mono_HLA-treated and CD14 Mono_Activated cells. The negative regulation of the MHC class II biosynthetic process was activated in CD14 Mono_Activated cells. In summary, the functions of LRP1 in the brain and blood are similar.

Charting the Regulatory Role of Lrp1 in Liver Diversity During AD Progression

Previous research revealed that LRP1 is not only abundant in the blood but also highly expressed in the liver, particularly after exercise, where liver Lrp1 levels significantly increase[17, 35]. Therefore, after quality control, we utilized the scRNA-seq dataset to determine the regulatory role of Lrp1 in the liver, which included 12,961 cells[20]. The linages were annotated based on the Seurat R package (version 4.4.0). We observed six distinct cell clusters in the liver (Fig. 4A). with LRP1 showing notable expression in monocytes and macrophages, hinting at their key role in AD progression (Fig. 4B). Consequently, we

focused on the function of Lrp1 in monocytes and macrophages. A T test revealed that, compared to that in the sedentary condition group, LRP1 expression was significantly greater in the exercise group ($P =$ 9.63e-05) (Fig. 4C). To further investigate the impact of exercise, we compared monocyte and macrophage counts between exercise and sedentary mice using FindMarkers and identified 349 DEGs (log2FC > 0.5, cell proportion > 0.3), 255 of which were upregulated and 94 of which were downregulated (Fig. 4D). We conducted enrichment analysis of these genes and discovered that the Lrp1-related functions included receptor-mediated endocytosis and Aβ protein clearance (Fig. 4G). To further explore the molecular interactions, we further explored the PPI interactions of the DEGs among the AD-related genes (Fig. 4E-F) and found that the upregulated submodules were associated mainly with Aβ protein clearance, negative regulation of cell death, and immune-related functions, while the downregulated submodules were related to oxidative phosphorylation and ALS (Fig. 4E). Notably, the PPI analysis highlighted the connection between Lrp1 and APP (Fig. 4F), suggesting that their interaction could be used in therapeutic strategies for Aβ protein phagocytosis in AD.

The Function of LRP1 in Multi-Tissue Contexts

In the previous sections, we summarized the functions of LRP1 in FC, PBMC, and the liver; however, the heterogeneity among these tissues has not been determined. To address this issue, we explored the heterogeneity and similarities of LRP1 functions across multi-tissue (Fig. 5A-B). After enriching for LRP1 functions across multi-tissue, we discovered that the functional changes induced by high LRP1 expression are highly similar and are primarily associated with Aβ protein clearance and phagocytosis (Fig. 5A). Additionally, in the learning or memory module, Stage 5 in the FC was highly enriched, whereas it was not enriched in Stage 1; furthermore, this function showed a smaller p value in exercise samples of the liver than in sedentary samples (Fig. 5B). These findings suggest that in the early stages of AD, phagocytic ability is greater than in the later stages. However, exercise can enhance cognitive ability and phagocytic capacity.

Previous research has shown that astrocyte and microglial LRP1 in the brain play a role in phagocytizing Aβ proteins[13, 36, 37], consistent with our findings from single-cell transcriptomic analysis. However, there is a gap in the literature regarding whether LRP1 in the liver has a similar role in phagocytizing Aβ proteins. To bridge this gap, we conducted a three-month aerobic exercise intervention on male C57BL6 wild-type mice and APP/PS1 mice to verify the role of liver LRP1 in AD. The results showed that, compared to the sedentary group, the exercise group exhibited improved cognitive abilities (Supplementary Fig. 2) and a significant reduction in brain Aβ deposition levels (Supplementary Fig. 3). Furthermore, Western blot experiments were specifically performed on the livers of the four groups of mice (Fig. 5C). Significant differences in liver LRP1 and Aβ levels were found among the four groups (F = 108.4, $P = 0.0003$ and F = 221.6, $P < 0.0001$). Notably, compared to those in the WTC group, the LRP1 levels in the WTE group were significantly greater ($P = 0.0257$). Similarly, the ADE group had a significantly greater level of LRP1 than the apparent diffusion coefficient (ADC) group ($P = 0.006$). Additionally, the Aβ levels in the WTE group were significantly greater than those in the WTC group ($P = 0.0035$), and the Aβ levels were significantly greater in the ADE group than in the ADC group ($P = 0.0145$)

(Fig. 5D). To further investigate this phenomenon, we conducted an Aβ uptake assay to confirm the phagocytic effect of liver LRP1 on Aβ proteins (Fig. 5E). The results showed a significant decrease in the level of Aβ proteins phagocytosed by macrophages after LRP1 knockdown ($P = 0.0022$) (Fig. 5F). These comprehensive findings strongly support our single-cell transcriptomic analysis, demonstrating the crucial role of macrophage LRP1 in the liver in the phagocytosis of Aβ proteins. In summary, exercise can enhance learning and memory in APP/PS1 mice to some extent, potentially through the exercise-induced upregulation of LRP1, which leads to increased phagocytosis of the Aβ protein.

Discussion

In this study, we observed alterations in the expression of LRP1 across various cell types and multi-tissue in AD, providing new insights into the role of LRP1 in AD. Initially, we focused on the FC, a critical region for AD pathology, where LRP1 is predominantly enriched in astrocyte, microglia, and OPCs. In astrocyte, LRP1 is mainly concentrated in A0 and plays a significant role in inflammation, neurodevelopment, and endocytosis. Similarly, in microglia, LRP1 is also predominantly expressed in M0 macrophages, which aligns with previous findings that LRP1 is involved primarily in phagocytosis and neurodevelopment[38–42]. Our novel contribution is to demonstrate that the absence of LRP1 in astrocyte and microglia impairs their ability to phagocytose Aβ proteins. Consequently, this impairment leads to the accumulation of Aβ proteins in the brain, which increases inflammatory responses in astrocyte and microglia, significantly impacting neurodevelopment. Consequently, these factors not only worsen the brain's physiological environment but also impair cognitive abilities. Furthermore, LRP1 engages in the phagocytosis of Aβ proteins and plays a key role in regulating tau protein endocytosis in neurons, which is crucial for the spread of tau proteins in the brain. Additionally, our research revealed that the A0 and M0 cell subsets interact mainly through the APP-CD74 pathway, with CD74 being identified as binding to amyloid precursor protein (APP) and inhibiting the production of Aβ[34]. Therefore, the APP-CD74 interaction not only aids in the phagocytosis of Aβ but also inhibits its production, contributing to a reduction in Aβ in the brain. In this context, proteins targeted by LRP1-mediated phagocytosis are likely degraded via lysosomal pathways. Recent studies suggest that microglia can phagocytose Aβ proteins through multiple pathways, with lysosomes further coordinating Aβ clearance[43, 44]. However, studies have reported conflicting data on the levels of LRP1 in the brains of AD patients. Several groups have noted increased levels of LRP1 mRNA in the temporal cortex and hippocampus of AD patients or individuals with dementia[45, 46], while others have observed decreased LRP1 mRNA expression in the frontal cortex of AD patients[47]. We propose that this inconsistency is due to the differential expression of LRP1 in various cell types[48]. Our findings clarify this phenomenon by revealing that LRP1 is found primarily in astrocyte, microglia, and OPCs. Moreover, by analyzing LRP1 expression levels at different stages of AD, we observed an increase in the early stages and a decrease in the later stages of AD. These findings further explain the variability of previous research results and underscore the importance of the timing of AD sample collection. In essence, LRP1 serves as a common factor that may underlie the cooccurrence of Aβ and tau pathologies.

Moreover, LRP1 plays a crucial role in maintaining the normal function of the blood brain barrier (BBB). Previous research has shown that ablation of brain endothelial LRP1 results in protease-mediated degradation of tight junctions, a reduction in P-glycoprotein (P-gp), and a loss of BBB integrity[49]. In this scenario, LRP1, which serves as a primary functional carrier of Aβ, significantly influences the efflux of Aβ from the brain to peripheral blood. Specifically, inside the brain, Aβ initially forms a complex with LRP1 ligands, binds to LRP1, leads to phosphorylation of the LRP1 tail, and becomes internalized to form endosomes. These proteins are subsequently transported through the BBB to peripheral blood[50]. In the peripheral nervous system, LRP1 is soluble LRP1 (sLRP1), the main protein that binds to Aβ in peripheral tissues and can bind approximately 90% of soluble Aβ. Consequently, this interaction results in the formation of a complex that cannot re-enter the brain through the BBB and is cleared by the liver and kidneys. Our research revealed that sLRP1 is highly enriched in monocytes in the blood, and its associated genes are involved mainly in acute inflammation, phagocytosis, and clearance of apoptotic cells. These findings highlight the role of sLRP1 in the blood. Furthermore, we observed that LRP1 levels in the liver significantly increase after exercise, enhancing the capacity of the liver to clear Aβ proteins. We discovered that LRP1 is primarily enriched in macrophages and monocytes in the liver. Interestingly, monocytes are present in the blood, but they migrate to the liver and transform into macrophages upon immune system regulation. To confirm these findings, we conducted in vivo and in vitro experiments and revealed that exercise mainly induces the upregulation of LRP1 in liver macrophages, thereby enhancing the phagocytosis of Aβ in the peripheral circulatory system. Additionally, our study showed that LRP1 in the liver is regulated primarily by Egr1 and Irf7 (Supplementary Fig. 4). Notably, previous research has identified Egr1 as an upregulator of the AD presenilin-2 gene in neuronal cells. Presenilin-2 is a component of the gamma-secretase complex involved in the processing of amyloid precursor protein (APP)[51]. These findings indicate that Egr1 could be a new target for AD treatment.

In our research, we found that LRP1 is predominantly enriched in liver monocytes or macrophages; in monocytes in the blood; and in microglia, astrocyte, and OPCs in the brain. This difference in prevalence across various immune-related cell types underscores the significant correlation between LRP1 and the immune system. Recent advancements in studies have further revealed the role of LRP1 in mediating immune functions[52]. For instance, LRP1 modulates the microglial immune response through the regulation of the JNK and NF-κB signaling pathways[53], actively contributes to neuroinflammation via OPCs[54], and mediates the immunosuppression of monocytes by α-MMCs[39]. Taken together, these examples collectively highlight the critical role of LRP1 in immune regulation. Importantly, enhancing immune function is highly beneficial not only for AD patients, as evidenced by multiple studies[55–57] but also for the general population[58, 59]. Therefore, exploring the molecular mechanisms involved in treating AD, especially from an immunological perspective, is vital for future research.

Conclusions

This study represents a significant advancement in understanding the role of LRP1 in AD, uncovering its multifaceted functions across multi-tissue at the single-cell level. Our findings not only corroborate previous findings about the involvement of LRP1 in AD pathology but also extend these findings by

revealing tissue-specific roles and delineating the influence of lifestyle factors such as physical activity. There are manifold implications of our research, revealing new perspectives for multidisciplinary approaches in AD research spanning molecular biology, neurology, and beyond. Our study bridges critical gaps in the literature by providing a detailed, single-cell view of the role of LRP1 in AD and challenging and refining current models of disease pathogenesis. The insights gained here not only open avenues for the development of novel therapeutic strategies targeting LRP1 but also suggest potential biomarkers for early AD diagnosis and progression monitoring. As the global prevalence of AD continues to increase, our findings are timely and contribute to the broader understanding of the molecular underpinnings of this disease. Consequently, this knowledge is crucial for developing public health strategies and enhancing the quality of life for individuals affected by AD. While our study provides comprehensive insights, it also underscores the complexity of AD and the need for further research. Therefore, future studies should focus on elucidating the exact mechanisms by which LRP1 influences AD progression and exploring how these pathways might be modulated for therapeutic benefit.

Abbreviations

LRP1
low-density lipoprotein receptor-related protein 1
AD
Alzheimer's Disease
Aβ
Amyloid-β
PCA
Principal component analysis
DEGs
Differentially expressed genes
KEGG
Kyoto Encyclopedia of Genes and Genomes
GSVA
Gene set variation analysis
AUC
Area under the curve
OPC
Oligodendrocyte progenitor cell
FC
Prefrontal cortex
UMAP
Uniform manifold approximation and projection
GO
Gene Ontology

GSEA

Gene set enrichment analysis

PBMC

Peripheral blood mononuclear cell

PCA

Principal component analysis

NOR

Novel object recognition

APP

amyloid precursor protein

BBB

Blood brain barrier

MWM

Morris water maze

SLRP1

Soluble LRP1

Declarations

Availability of data and materials

Single-cell data can be accessed via the GSE181279 https://www.ncbi.nlm.nih.gov/geo/query/acc.cgi?acc=GSE181279, GSE174367 https://www.ncbi.nlm.nih.gov/geo/query/acc.cgi?acc=GSE174367, and GSE173429 https://www.ncbi.nlm.nih.gov/geo/query/acc.cgi?acc=GSE173429 datasets.

Acknowledgments

Not applicable.

Author information

Kang Chen and Zilin Wei shared the first authorship.

Authors and affiliations

Institute of Environmental and Operational Medicine, Academy of Military Medical Sciences, Academy of Military Sciences, Tianjin, China

Kang Chen, ZiLin Wei, AiLi Wei, YingKai Qin, Chen Liu, Haolin Xin, Shisheng Chen, Kun Wang, TianHui Wang

Tianjin Key Laboratory of Exercise Physiology & Sports Medicine, Tianjin University of Sport, Tianjin, China

Kang Chen, Chen Liu, Haolin Xin, Shisheng Chen

Information Center of Logistics Support Department of CMC, Beijing, China

Yi Ge

No. 950 Hospital of the Chinese People's Liberation Army, Yecheng, China

Bin Li

Contributions

C K and W ZL designed the study and wrote the paper. The data were analyzed by C K, W ZL, W AL, Q YK, L C, C SS, X HL, G Y, L B, W K and W TH. Animal experiments were conducted by C K, W ZL, W AL, Q YK, L C, C SS, X HL, W K and W TH. Histopathological analyses were also conducted by C K, W ZL, W AL, Q YK, L C, C SS, X HL, G Y, L B, W K and W TH. All the authors have read and approved the final manuscript.

Corresponding author

Correspondence to Kun Wang or TianHui Wang

813073768@qq.com (Kun Wang); wydny668@163.com (TianHui Wang)

Ethics declarations

Ethics approval and consent to participate

The animal study protocol was approved by the Institutional Animal Care and Use Committee (IACUC) of the Chinese Academy of Military Medical Science.

Consent for publication

Not applicable.

Competing interests

The authors declare that they do not have any competing interests.

References

1. Scheltens P, Blennow K, Breteler MM, et al. Alzheimer's disease. *Lancet* 2016; 388: 505-517. 2016/02/28. DOI: 10.1016/S0140-6736(15)01124-1.

2. Scheltens P, De Strooper B, Kivipelto M, et al. Alzheimer's disease. *Lancet* 2021; 397: 1577-1590. 2021/03/06. DOI: 10.1016/S0140-6736(20)32205-4.

3. Goedert M and Spillantini MG. A century of Alzheimer's disease. *Science* 2006; 314: 777-781. 2006/11/04. DOI: 10.1126/science.1132814.

4. LaFerla FM and Oddo S. Alzheimer's disease: Abeta, tau and synaptic dysfunction. *Trends Mol Med* 2005; 11: 170-176. 2005/04/13. DOI: 10.1016/j.molmed.2005.02.009.

5. Hampel H, Hardy J, Blennow K, et al. The Amyloid-beta Pathway in Alzheimer's Disease. *Mol Psychiatry* 2021; 26: 5481-5503. 2021/08/31. DOI: 10.1038/s41380-021-01249-0.

6. Nakanishi K, Sakakima H, Norimatsu K, et al. Effect of low-intensity motor balance and coordination exercise on cognitive functions, hippocampal Abeta deposition, neuronal loss, neuroinflammation, and oxidative stress in a mouse model of Alzheimer's disease. *Exp Neurol* 2021; 337: 113590. 2021/01/04. DOI: 10.1016/j.expneurol.2020.113590.

7. Jawhar S, Trawicka A, Jenneckens C, et al. Motor deficits, neuron loss, and reduced anxiety coinciding with axonal degeneration and intraneuronal Abeta aggregation in the 5XFAD mouse model of Alzheimer's disease. *Neurobiol Aging* 2012; 33: 196 e129-140. 2010/07/14. DOI: 10.1016/j.neurobiolaging.2010.05.027.

8. Cheng Y, Tian DY and Wang YJ. Peripheral clearance of brain-derived Abeta in Alzheimer's disease: pathophysiology and therapeutic perspectives. *Transl Neurodegener* 2020; 9: 16. 2020/05/10. DOI: 10.1186/s40035-020-00195-1.

9. Nalivaeva NN and Turner AJ. Targeting amyloid clearance in Alzheimer's disease as a therapeutic strategy. *Br J Pharmacol* 2019; 176: 3447-3463. 2019/02/03. DOI: 10.1111/bph.14593.

10. Fan Z, Ren T, Wang Y, et al. Abeta-responsive metformin-based supramolecular synergistic nanodrugs for Alzheimer's disease by enhancing microglial Abeta clearance. *Biomaterials* 2022; 283: 121452. 2022/03/15. DOI: 10.1016/j.biomaterials.2022.121452.

11. van de Sluis B, Wijers M and Herz J. News on the molecular regulation and function of hepatic low-density lipoprotein receptor and LDLR-related protein 1. *Curr Opin Lipidol* 2017; 28: 241-247. 2017/03/17. DOI: 10.1097/MOL.0000000000000411.

12. Gerritsen KG, Bovenschen N, Nguyen TQ, et al. Rapid hepatic clearance of full length CCN-2/CTGF: a putative role for LRP1-mediated endocytosis. *J Cell Commun Signal* 2016; 10: 295-303. 2016/09/21. DOI: 10.1007/s12079-016-0354-6.

13. Liu CC, Hu J, Zhao N, et al. Astrocytic LRP1 Mediates Brain Abeta Clearance and Impacts Amyloid Deposition. *J Neurosci* 2017; 37: 4023-4031. 2017/03/10. DOI: 10.1523/JNEUROSCI.3442-16.2017.

14. Van Gool B, Storck SE, Reekmans SM, et al. LRP1 Has a Predominant Role in Production over Clearance of Abeta in a Mouse Model of Alzheimer's Disease. *Mol Neurobiol* 2019; 56: 7234-7245. 2019/04/21. DOI: 10.1007/s12035-019-1594-2.

15. Storck SE, Meister S, Nahrath J, et al. Endothelial LRP1 transports amyloid-beta(1-42) across the blood−brain barrier. *J Clin Invest* 2016; 126: 123-136. 2015/12/01. DOI: 10.1172/JCI81108.

16. Pflanzner T, Janko MC, Andre-Dohmen B, et al. LRP1 mediates bidirectional transcytosis of amyloid-beta across the blood−brain barrier. *Neurobiol Aging* 2011; 32: 2323 e2321-2311. 2010/07/16. DOI: 10.1016/j.neurobiolaging.2010.05.025.

17. Khodadadi D, Gharakhanlou R, Naghdi N, et al. Treadmill Exercise Ameliorates Spatial Learning and Memory Deficits Through Improving the Clearance of Peripheral and Central Amyloid-Beta Levels. *Neurochem Res* 2018; 43: 1561-1574. 2018/06/28. DOI: 10.1007/s11064-018-2571-2.

18. Xu H and Jia J. Single-Cell RNA Sequencing of Peripheral Blood Reveals Immune Cell Signatures in Alzheimer's Disease. *Front Immunol* 2021; 12: 645666. 2021/08/28. DOI: 10.3389/fimmu.2021.645666.

19. Morabito S, Miyoshi E, Michael N, et al. Single-nucleus chromatin accessibility and transcriptomic characterization of Alzheimer's disease. *Nat Genet* 2021; 53: 1143-1155. 2021/07/10. DOI: 10.1038/s41588-021-00894-z.

20. Zhang H, Chen T, Ren J, et al. Preoperative exercise therapy triggers anti-inflammatory trained immunity of Kupffer cells through metabolic reprogramming. *Nat Metab* 2021; 3: 843-858. 2021/06/16. DOI: 10.1038/s42255-021-00402-x.

21. Hao Y, Hao S, Andersen-Nissen E, et al. Integrated analysis of multimodal single-cell data. *Cell* 2021; 184: 3573-3587 e3529. 2021/06/02. DOI: 10.1016/j.cell.2021.04.048.

22. Aran D, Looney AP, Liu L, et al. Reference-based analysis of lung single-cell sequencing reveals a transitional profibrotic macrophage. *Nat Immunol* 2019; 20: 163-172. 2019/01/16. DOI: 10.1038/s41590-018-0276-y.

23. Yu G, Wang LG, Han Y, et al. clusterProfiler: an R package for comparing biological themes among gene clusters. *OMICS* 2012; 16: 284-287. 2012/03/30. DOI: 10.1089/omi.2011.0118.

24. Hanzelmann S, Castelo R and Guinney J. GSVA: gene set variation analysis for microarray and RNA-seq data. *BMC Bioinformatics* 2013; 14: 7. 2013/01/18. DOI: 10.1186/1471-2105-14-7.

25. Wickham H and Wickham H. *Data analysis*. Springer, 2016.

26. Jin S, Guerrero-Juarez CF, Zhang L, et al. Inference and analysis of cell−cell communication using CellChat. *Nat Commun* 2021; 12: 1088. 2021/02/19. DOI: 10.1038/s41467-021-21246-9.

27. Huynh-Thu VA, Irrthum A, Wehenkel L, et al. Inferring regulatory networks from expression data using tree-based methods. *PLoS One* 2010; 5 2010/10/12. DOI: 10.1371/journal.pone.0012776.

28. Xie Y, Wu Z, Sun L, et al. Swimming exercise reverses chronic unpredictable mild stress-induced depression-like behaviors and alleviates neuroinflammation and collapsing response mediator protein-2-mediated neuroplasticity injury in adult male mice. *Neuroreport* 2022; 33: 272-282. 2022/04/07. DOI: 10.1097/WNR.0000000000001779.

29. Bellaver B, Povala G, Ferreira PCL, et al. Astrocyte reactivity influences amyloid-beta effects on tau pathology in preclinical Alzheimer's disease. *Nat Med* 2023; 29: 1775-1781. 2023/05/30. DOI: 10.1038/s41591-023-02380-x.

30. Ju YH, Bhalla M, Hyeon SJ, et al. Astrocytic urea cycle detoxifies Abeta-derived ammonia while impairing memory in Alzheimer's disease. *Cell Metab* 2022; 34: 1104-1120 e1108. 2022/06/24. DOI:

10.1016/j.cmet.2022.05.011.

31. Floden AM and Combs CK. Microglia demonstrate age-dependent interaction with amyloid-beta fibrils. *J Alzheimers Dis* 2011; 25: 279-293. 2011/03/16. DOI: 10.3233/JAD-2011-101014.

32. Hänzelmann S, Castelo R and Guinney JJBb. GSVA: gene set variation analysis for microarray and RNA-seq data. 2013; 14: 1-15.

33. Yuan J, Wang J, Jiang Q, et al. Identification of Novel Lung Adenocarcinoma Subtypes and Prognostic Gene Sets Based on GSVA Analysis. 2023.

34. Matsuda S, Matsuda Y and D'Adamio L. CD74 interacts with APP and suppresses the production of Abeta. *Mol Neurodegener* 2009; 4: 41. 2009/10/24. DOI: 10.1186/1750-1326-4-41.

35. Storck SE and Pietrzik CU. Endothelial LRP1 - A Potential Target for the Treatment of Alzheimer's Disease : Theme: Drug Discovery, Development and Delivery in Alzheimer's Disease Guest Editor: Davide Brambilla. *Pharm Res* 2017; 34: 2637-2651. 2017/09/28. DOI: 10.1007/s11095-017-2267-3.

36. Rauch JN, Luna G, Guzman E, et al. LRP1 is a master regulator of tau uptake and spread. *Nature* 2020; 580: 381-385. 2020/04/17. DOI: 10.1038/s41586-020-2156-5.

37. He Y, Ruganzu JB, Jin H, et al. LRP1 knockdown aggravates Abeta(1-42)-stimulated microglial and astrocytic neuroinflammatory responses by modulating TLR4/NF-kappaB/MAPKs signaling pathways. *Exp Cell Res* 2020; 394: 112166. 2020/07/10. DOI: 10.1016/j.yexcr.2020.112166.

38. Hansen DV, Hanson JE and Sheng M. Microglia in Alzheimer's disease. *J Cell Biol* 2018; 217: 459-472. 2017/12/03. DOI: 10.1083/jcb.201709069.

39. Jorfi M, Maaser-Hecker A and Tanzi RE. The neuroimmune axis of Alzheimer's disease. *Genome Med* 2023; 15: 6. 2023/01/27. DOI: 10.1186/s13073-023-01155-w.

40. Fakhoury M. Microglia and Astrocyte in Alzheimer's Disease: Implications for Therapy. *Curr Neuropharmacol* 2018; 16: 508-518. 2017/07/22. DOI: 10.2174/1570159X15666170720095240.

41. Sadick JS, O'Dea MR, Hasel P, et al. Astrocyte and oligodendrocytes undergo subtype-specific transcriptional changes in Alzheimer's disease. *Neuron* 2022; 110: 1788-1805 e1710. 2022/04/06. DOI: 10.1016/j.neuron.2022.03.008.

42. Johnson ECB, Dammer EB, Duong DM, et al. Large-scale proteomic analysis of Alzheimer's disease brain and cerebrospinal fluid reveals early changes in energy metabolism associated with microglia and astrocyte activation. *Nat Med* 2020; 26: 769-780. 2020/04/15. DOI: 10.1038/s41591-020-0815-6.

43. Jantti H, Sitnikova V, Ishchenko Y, et al. Microglial amyloid beta clearance is driven by PIEZO1 channels. *J Neuroinflammation* 2022; 19: 147. 2022/06/16. DOI: 10.1186/s12974-022-02486-y.

44. Shi Q, Chang C, Saliba A, et al. Microglial mTOR Activation Upregulates Trem2 and Enhances beta-Amyloid Plaque Clearance in the 5XFAD Alzheimer's Disease Model. *J Neurosci* 2022; 42: 5294-5313. 2022/06/08. DOI: 10.1523/JNEUROSCI.2427-21.2022.

45. Matsui T, Ingelsson M, Fukumoto H, et al. Expression of APP pathway mRNAs and proteins in Alzheimer's disease. *Brain Res* 2007; 1161: 116-123. 2007/06/26. DOI:

10.1016/j.brainres.2007.05.050.

46. Akram A, Schmeidler J, Katsel P, et al. Association of ApoE and LRP mRNA levels with dementia and AD neuropathology. *Neurobiol Aging* 2012; 33: 628 e621-628 e614. 2011/06/17. DOI: 10.1016/j.neurobiolaging.2011.04.010.

47. Yamanaka Y, Faghihi MA, Magistri M, et al. Antisense RNA controls LRP1 Sense transcript expression through interaction with a chromatin-associated protein, HMGB2. *Cell Rep* 2015; 11: 967-976. 2015/05/06. DOI: 10.1016/j.celrep.2015.04.011.

48. Storck SE, Kurtyka M and Pietrzik CU. Brain endothelial LRP1 maintains blood−brain barrier integrity. *Fluids Barriers CNS* 2021; 18: 27. 2021/06/21. DOI: 10.1186/s12987-021-00260-5.

49. Yamada K, Hashimoto T, Yabuki C, et al. The low density lipoprotein receptor-related protein 1 mediates uptake of amyloid beta peptides in an in vitro model of the blood−brain barrier cells. *J Biol Chem* 2008; 283: 34554-34562. 2008/10/23. DOI: 10.1074/jbc.M801487200.

50. Yang L, Liu CC, Zheng H, et al. LRP1 modulates the microglial immune response via regulation of JNK and NF-kappaB signaling pathways. *J Neuroinflammation* 2016; 13: 304. 2016/12/10. DOI: 10.1186/s12974-016-0772-7.

51. Hu YT, Chen XL, Huang SH, et al. Early growth response-1 regulates acetylcholinesterase and its relation with the course of Alzheimer's disease. *Brain Pathol* 2019; 29: 502-512. 2018/12/05. DOI: 10.1111/bpa.12688.

52. Sizova O, John LS, Ma Q, et al. Multifaceted role of LRP1 in the immune system. *Front Immunol* 2023; 14: 1166189. 2023/04/07. DOI: 10.3389/fimmu.2023.1166189.

53. Fernandez-Castaneda A, Chappell MS, Rosen DA, et al. The active contribution of OPCs to neuroinflammation is mediated by LRP1. *Acta Neuropathol* 2020; 139: 365-382. 2019/09/26. DOI: 10.1007/s00401-019-02073-1.

54. Deng N, Li M, Shen D, et al. LRP1 receptor-mediated immunosuppression of alpha-MMC on monocyte. *Int Immunopharmacol* 2019; 70: 80-87. 2019/02/21. DOI: 10.1016/j.intimp.2019.01.036.

55. Su W, Saravia J, Risch I, et al. CXCR6 orchestrates brain CD8(+) T-cell residency and limits mouse Alzheimer's disease pathology. *Nat Immunol* 2023; 24: 1735-1747. 2023/09/08. DOI: 10.1038/s41590-023-01604-z.

56. Suzzi S, Croese T, Ravid A, et al. N-acetylneuraminic acid links immune exhaustion and accelerated memory deficit in diet-induced obese Alzheimer's disease mouse model. *Nat Commun* 2023; 14: 1293. 2023/03/10. DOI: 10.1038/s41467-023-36759-8.

57. Chen HY, Zhao Y and Xie YZ. Immunosenescence of brain accelerates Alzheimer's disease progression. *Rev Neurosci* 2023; 34: 85-101. 2022/07/06. DOI: 10.1515/revneuro-2022-0021.

58. Mazziotta C, Tognon M, Martini F, et al. Probiotics Mechanism of Action on Immune Cells and Beneficial Effects on Human Health. *Cells* 2023; 12 2023/01/09. DOI: 10.3390/cells12010184.

59. Bieri G, Schroer AB and Villeda SA. Blood-to-brain communication in aging and rejuvenation. *Nat Neurosci* 2023; 26: 379-393. 2023/01/17. DOI: 10.1038/s41593-022-01238-8.
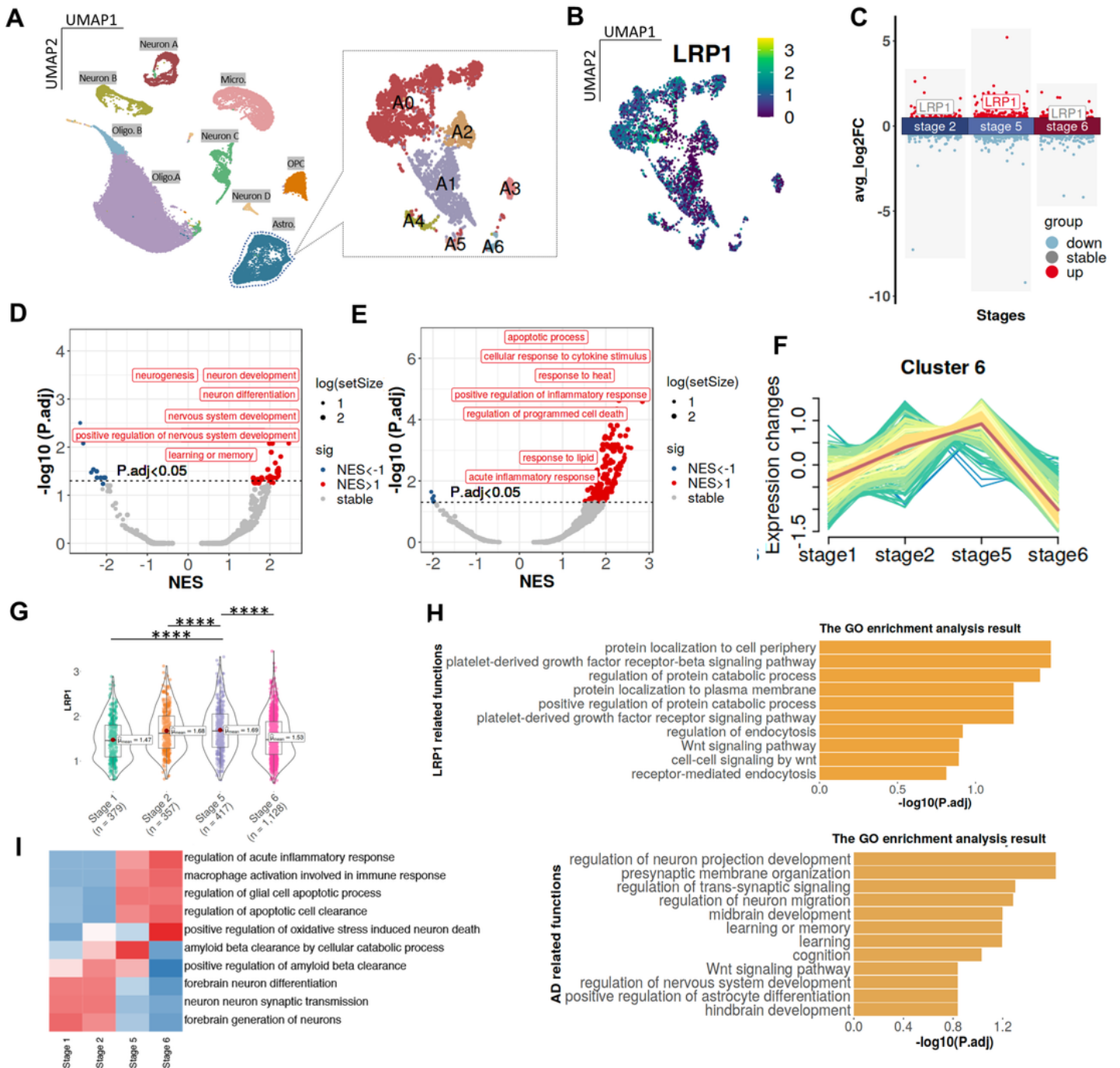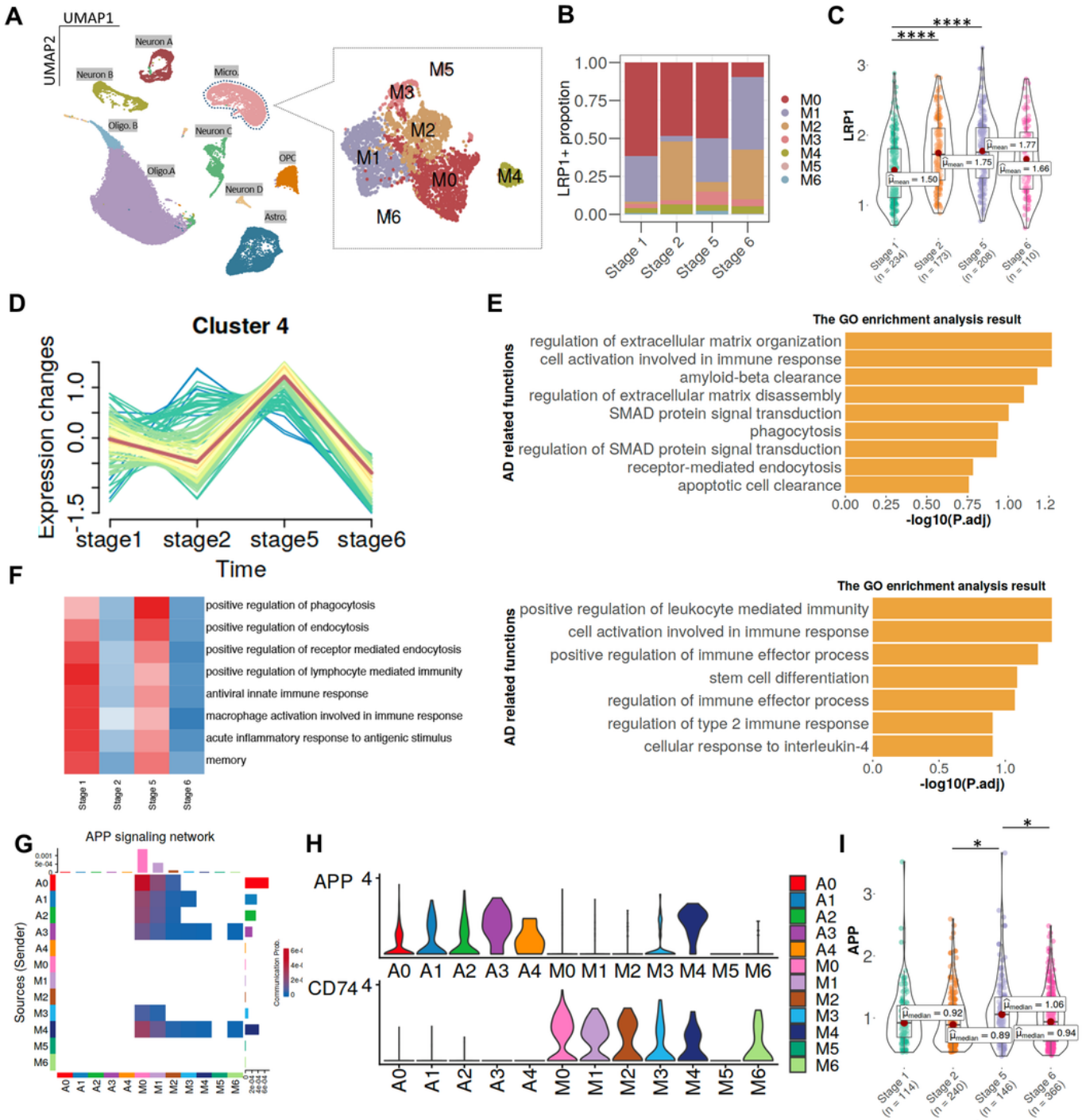
Figures

Figure 1

Uncovering the involved functions and intricate role of LRP1 in astrocyte during the progression of AD.

A UMAP clustering of FC cell types and astrocyte reclustering. **B** UMAP visualization of LRP1 expression in distinct cell clusters. **C** Changes in the expression of LRP1 across AD stages. **D** GSEA plot contrasting Stage 1 and Stage 5 gene sets. **E** GSEA plot contrasting Stage 1 and Stage 6 gene sets. **F** Mfuzz analysis of DEGs between Stage 1 and Stage 5. **G** LRP1 expression levels through different stages of AD. **H** GO enrichment analysis of genes differentially expressed between Stage 1 and Stage 5. **I** GSVA heatmaps of gene sets in the A0 astrocyte subset across AD stages. ****P<0.0001.

Figure 2

Uncovering the involved functions and intricate role of LRP1 in microglia during the progression of AD.

A UMAP clustering of FC cell types and microglial reclustering. **B** LRP1 expression in microglial subtypes. **C** LRP1 expression in the M0 subtype across AD stages. **D** Mfuzz clustering of genes differentially expressed between Stage 1 and Stage 5. **E** GO enrichment analysis of genes differentially expressed between Stage 5 and Stage 1. **F** GSVA heatmap for gene sets in the M0 subtype across stages of AD. **G** Heatmap of APP signaling network interactions between microglia and astrocyte. **H** Expression of APP and CD74 in microglial and astrocyte subtypes. **I** APP expression in the M0 subtype across stages of AD. *P<0.05, ****P<0.0001.
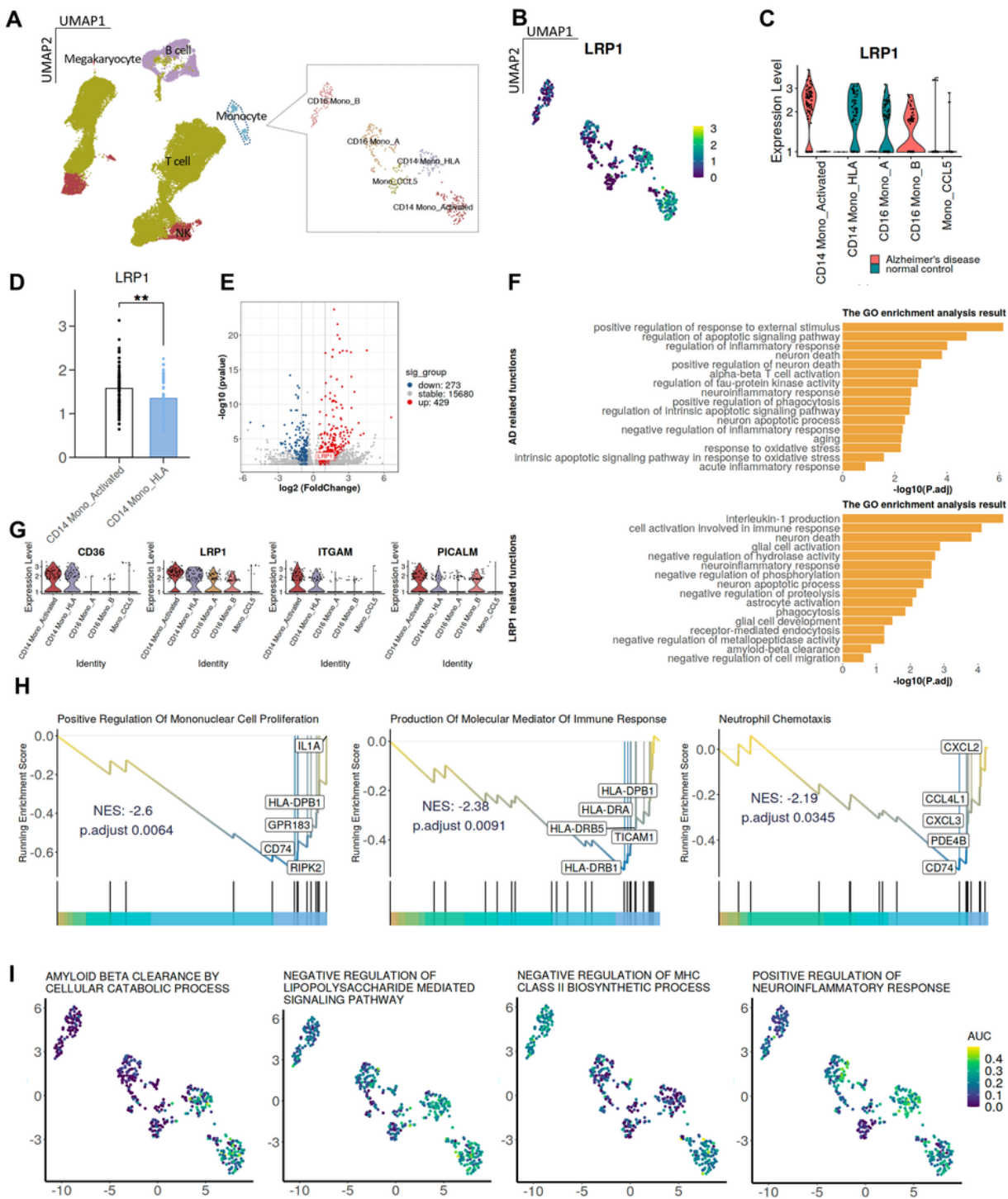
Figure 3

The functions and roles of LRP1 are similar between the brain and blood.

A UMAP clustering of PBMC cell types and monocyte reclustering. **B** UMAP visualization of LRP1 expression in distinct cell clusters. **C** Distribution of LRP1 expression across different cell clusters. **D** LRP1 expression in specific monocyte subsets and megakaryocytes. **E** Differentially expressed genes

between CD14 Mono_Activated and CD14 Mono_HLA genes. **F** GO term enrichment analysis of genes differentially expressed between CD14 Mono_Activated and CD14 Mono_HLA genes. **G** Gene expression profiles of phagocytosis-related genes in different cell clusters. **H** GSEA of genes differentially expressed between CD14 Mono_Activated and CD14 Mono_HLA genes. **I** AUCell analysis of genes differentially expressed between CD14 Mono_Activated and CD14 Mono_HLA genes.
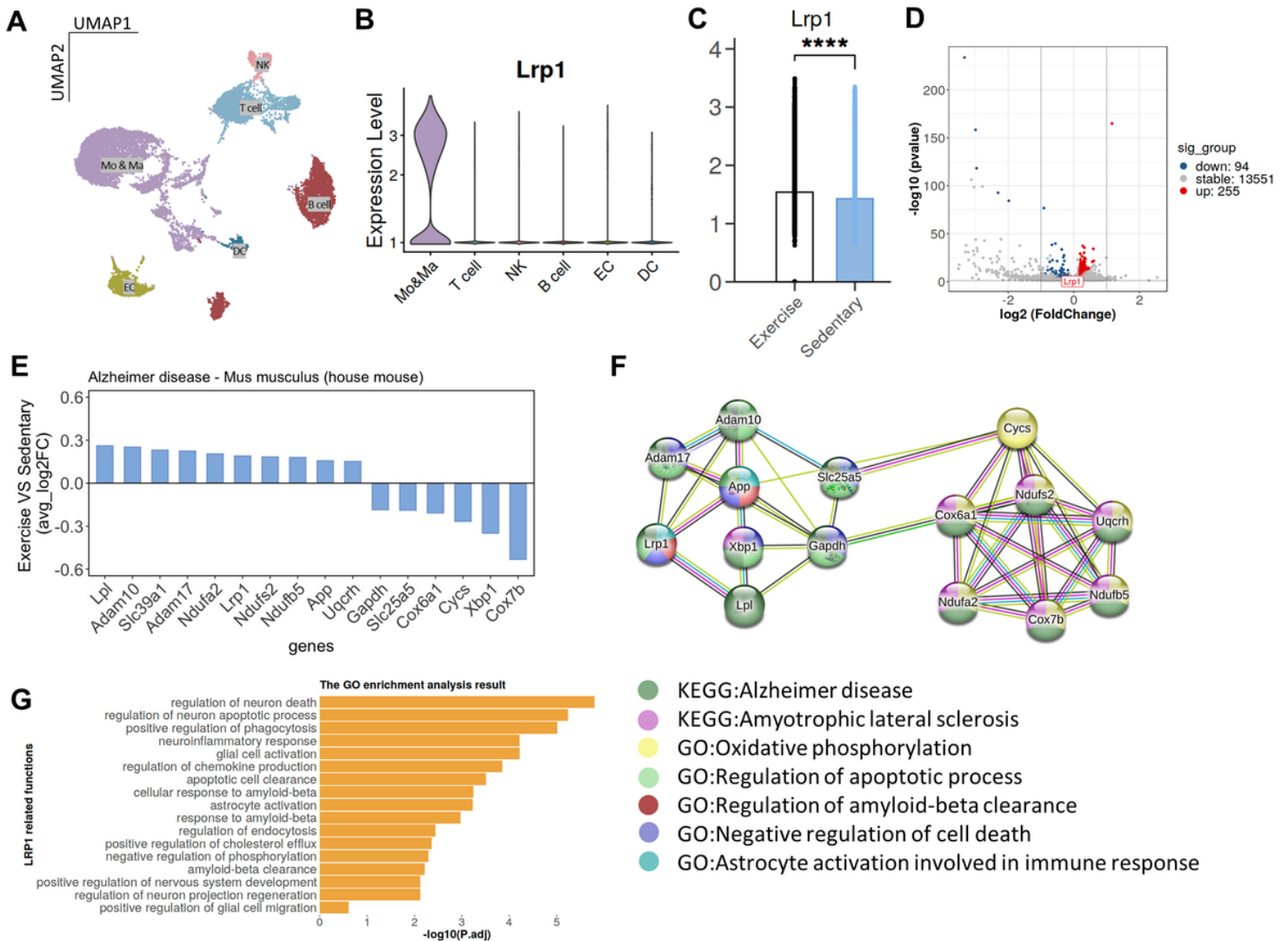

Figure 4

Exercise-induced upregulation of Lrp1 expression contributes to alleviating AD symptoms.

A UMAP clustering of liver cell types. **B** Lrp1 expression across different liver cell clusters. **C** Comparison of Lrp1 expression in monocytes and macrophages between sedentary conditions. **D.** Genes differentially expressed between exercise and sedentary conditions in monocytes and macrophages. **E** Differential expression of AD-related genes between monocytes and macrophages during exercise and sedentary conditions. **F** PPI network analysis of the genes shown in Fig. 4E. **G** GO enrichment analysis of genes

differentially expressed between exercised and sedentary mice among monocytes and macrophages.
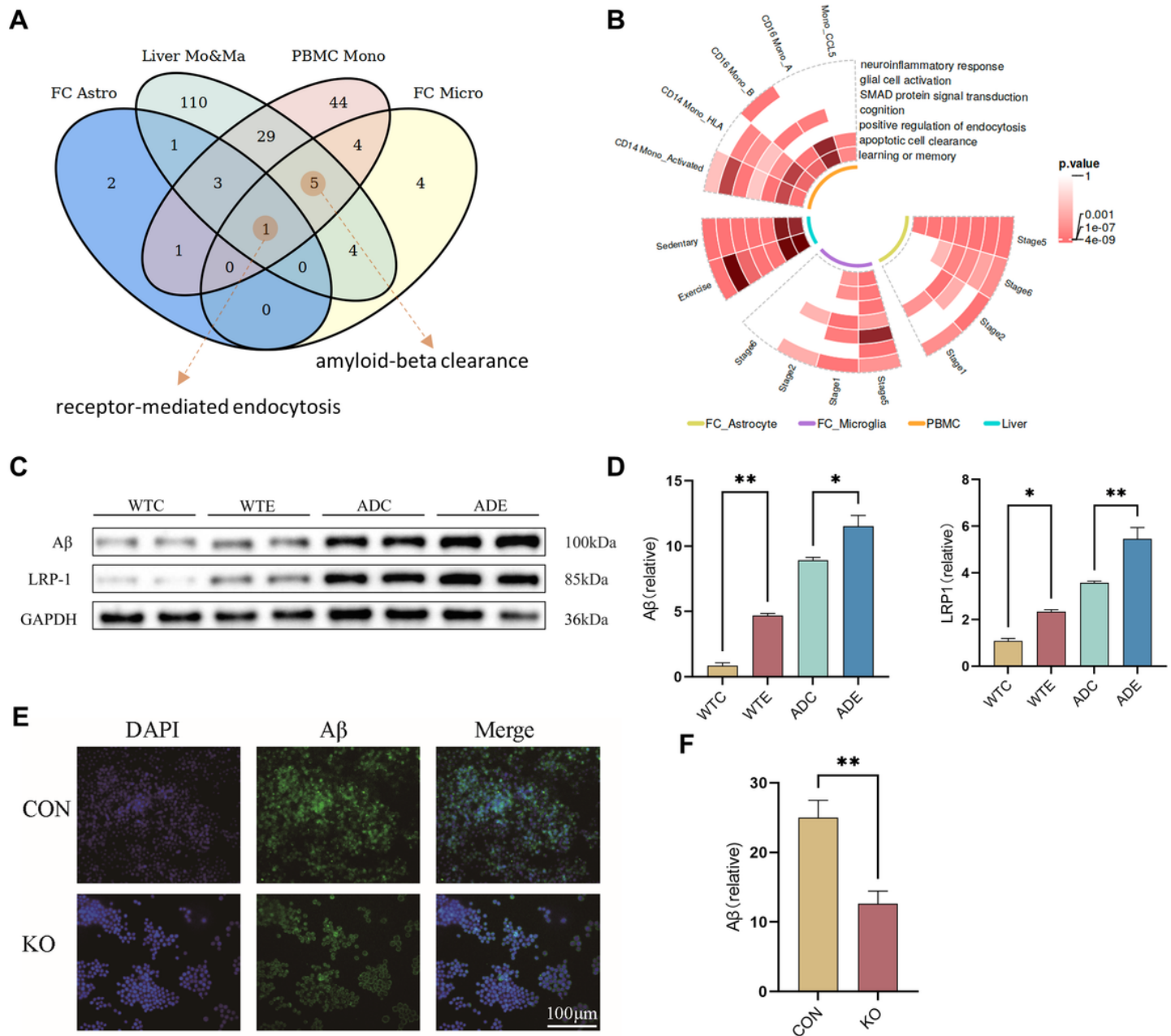****P<0.0001.

Figure 5

Integrative analysis suggested that LRP1 may enhance amyloid-beta clearance via endocytosis.

A Venn diagram of LRP1-related functional overlaps in multi-tissue. **B** The distribution of shared functions involving LRP1 across tissues. **C** Western blot bands for Aβ and LRP1 in control and exercised mouse liver samples. **D** Quantitative western blot analysis of the Aβ and LRP1 proteins. **E** Fluorescence

microscopy images of Aβ uptake in Kupffer cells with normal and reduced LRP1 levels. Scale bar =100 μm. **G:** Quantitative analysis of Aβ uptake efficiency in Kupffer cells. *P< 0.05, **P< 0.01.

Supplementary Files

This is a list of supplementary files associated with this preprint. Click to download.

- Supplementary.docx
- Graphicalabstract.png